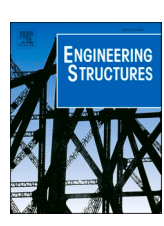
ELSEVIER

Contents lists available at ScienceDirect

Engineering Structures

journal homepage: www.elsevier.com/locate/engstruct



Backbone moment-rotation models for partial-strength steel endplate connections

Zizhou Ding, Ahmed Elkady

Department of Civil, Maritime and Environmental Engineering, University of Southampton, Burgess Road, Boldrewood Campus, Southampton SO16 7QF, UK

ARTICLE INFO

Keywords:
Steel joints
Nonlinear modeling
Finite element analysis
Moment-rotation response
Partial-strength endplate connections
Backbone curve
Modeling uncertainty

ABSTRACT

Phenomenological rotational spring models are critical components of system-level numerical simulations that employ the concentrated plasticity approach. These models must accurately capture the nonlinear behavior and degradation mechanisms in structural members and connections. Robust models for partial strength/semi-rigid steel flush and extended endplate connections are currently missing. Using the large amount of experimental data in the literature for endplate connections, complemented with parametric continuum finite element simulation, robust nonlinear models are developed. The models characterize the nonlinear monotonic backbone moment-rotation response up to failure as well as the post-failure response. The models achieve high accuracy metrics with 75 % of the data being predicted with an error of less than ± 10 %. Statistical metrics are also provided to quantify the model uncertainty. The regression-based models are consistent, in definition and format, with those found in existing modelling guidelines/standards such as ASCE 41. The proposed models support robust nonlinear analysis procedures, particularly as part of the performance-based evaluation, retrofit, and design framework.

1. Introduction

Lumped plasticity models are common in the assessment of buildings as part of the performance-based design framework and nonlinear analysis procedures that are becoming more popular in engineering practice. As part of these models, zero-length rotational springs are used to represent the nonlinear response of the different structural members and connections, at the expected location of the plastic zone. The springs are assigned to phenomenological mathematical models that characterize the component's monotonic/cyclic backbone response and cyclic deterioration parameters. [1-6]. The accuracy of such models is fundamental in acquiring accurate system-level simulations, efficient designs, and performance-based acceptance criteria. Towards that end, there has been significant progress towards the development of such models for steel frame buildings, including wide-flange columns. [7], hollow-section braces [8], column web-panel zone [9], shear-tab connections [10], and fully rigid beam-to-column connections [3]. Concerning partial-strength endplate steel connections, accurate nonlinear models, that capture the full response up to failure and their dependency on the connection's geometric and material properties, remain missing [11,12].

Partial-strength flush and extended steel endplate connections (referred to henceforth as FEPCs and EEPCs, respectively), shown in Fig. 1, are popular in construction practice worldwide [13–15]. Fig. 1 also shows the key geometric parameters of the two connection types that will be discussed in subsequent sections. The connections comprise a steel beam (I-shaped beams are considered herein) that is welded (mostly fillet weld is used) to an endplate and bolted to an I-shaped column's flange using high-strength bolts. In the case of EEPCs, the column flanges and the endplate may be further reinforced with horizontal stiffeners and rib plates, respectively. FEPCs are mostly found in gravity load-resisting systems in regions with low to high seismicity. EEPCs can further resist lateral loads such as wind and moderate earthquakes. In seismic regions, FEPCs are assumed to be part of a gravity load-resisting system whose contribution is usually ignored in seismic/wind design and simulation. This contribution was shown to be beneficial to the building response [10,16,17]; therefore, its exclusion is regarded as conservative and thusacceptable. Nonetheless, considering the true behavior of these connections, rather than idealizing them as pinned/fixed, will potentially produce accurate simulations, lead to robust structural response assessments, and efficient designs.

In both connections, endplate and column flange yielding due to

E-mail addresses: zd3e20@soton.ac.uk (Z. Ding), a.elkady@soton.ac.uk (A. Elkady).

 $^{^{\}ast}$ Corresponding author.

bending deformations are the most dominant damage modes. Although the former is sought in design over the latter to minimize column damage. Those two modes occur individually or combined depending on the relative thickness between the two components (i.e., $t_{\rm cf}$ and $t_{\rm ep}$) as illustrated in Fig. 2 for standard 4-bolt FEPC and 8-bolt EEPC. Other deformation modes can also take place simultaneously, such as column web (panel zone) shear, bolt elongation, and beam buckling. The latter is most likely to occur in borderline EEPCs that can achieve plastic strength close to (or exceeding) that of the beam.

Under monotonic loading, the connections develop a power-shaped moment-rotation curve with a rounded transition between the elastic and post-yield (hardening) slopes, as demonstrated in Fig. 3. Partialstrength endplate connections, and particularly FEPCs, are expected to reach relatively high levels of ductility in conjunction with their flexibility. Failure (complete loss of strength) generally occurs in a brittle manner in the form of weld fracture or bolt rupture. With proper weld design, detailing, and execution, weld failure can be avoided, leaving bolt rupture (under tension or combined tension/shear) as the primary failure mode. This is corroborated by past research [11,18]. Cyclically, the connections develop a pinched response due to the opening and closure of the gap between the endplate and the column flange. With respect to the bounding moment-rotation response, there is no major difference between the monotonic backbone curve and the cyclic envelope curve (see Fig. 3(a) and (b)). This is attributed to the absence of in-cycle strength deterioration, which is a result of the stable plastic cyclic behavior associated with endplate bending, column flange bending, bolt elongation, and/or panel zone shear. In-cycle strength degradation only occurs in limited cases where beam buckling is one of the deformation modes. In the absence of beam flange buckling, the small difference observed in moment rotation only relates to the cyclic material hardening properties. In that sense, partial-strength endplate connections do not experience load history dependency as observed in other structural components that experience unrestrained web/flange buckling, such as wide-flange beam-columns [19,20] and fully rigid welded/bolted beam-to-column connections [3,21]. This excludes ductility (i.e., failure rotation), which can be impacted by cyclic loading.

Considering the different possible deformation modes, predicting the moment-rotation response of partial-strength endplate connections can be challenging. There has been a relatively large effort in the literature to develop reliable models to predict the full moment-rotation response or the key response parameters (elastic rotation stiffness and plastic strength) of partial-strength steel connections, particularly endplate connections. The model types vary between empirical (traditional regression and machine learning models), semi-empirical, mechanical, and analytical. Recent comprehensive experimental-based evaluation studies [11,12] have assessed existing predictive models and showed that they are either too complex, have limited applicability range, produced large errors when assessed across the practical design space, or do not capture post-yield response (i.e., hardening and ultimate strength). Most importantly, no models are available for predicting the rotational ductility and post-failure response.

With this background, this paper aims to propose new generalized

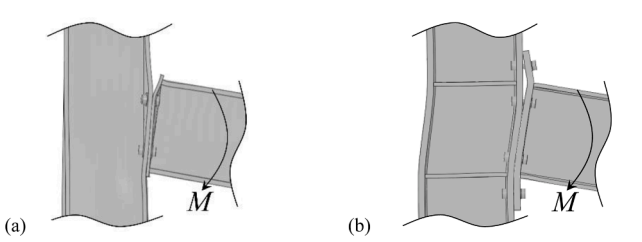


Fig. 2. General deformation mode in partial-strength (a) FEPCs and (b) EEPCs.

accurate models to characterize the full-range backbone moment-rotation behavior of partial-strength endplate connections, including failure and post-failure response. A large dataset is used for this purpose which includes available experimental data and supplemented by parametric continuum finite element simulations. This dataset is then used to develop simple empirical models, using traditional multivariate regression, to predict the backbone moment-rotation response parameters of FEPCs and EEPCs up to failure controlled by bolt rupture. The models aim to address the gap in existing modeling guidelines and support the ongoing effort to advance computational modeling for steel frame structures.

2. Regression dataset

A large dataset was assembled for developing the backbone models. This includes both experimental and simulation data. A total of 1159 specimens were used for FEPCs and 2296 for EEPCs. The dataset is concerned with bare steel beam-to-column joints with FEPCs or EEPCs and with/without column stiffeners. Connections with endplate stiffeners (ribs) and/or beam haunches are excluded; those are not commonly used in partial-strength EEPCs. Both EEPCs with double- and single-extended (on the tension side) endplates are considered.

The experimental data was obtained from a recently collated multi-attribute digital database [11,23]. A total of 239 test specimens were collected for FEPCs and 312 for EEPCs. This is a considerably larger amount of data compared to past attempts to develop empirical models [24,25]. The data encompass connections fabricated from different steel grades including mild, high-strength, and stainless steel. Fig. 4 shows the ranges of the column and beam heights ($h_{\rm c}$ and $h_{\rm b}$, respectively) as well as the column and endplate thicknesses covered by the experimental data.

Although the experimental data is well dispersed, parametric continuum finite element (CFE) simulations were conducted to further complement and fill the gaps within the experimental data. As inferred from Fig. 4, the parametric simulations help produce uniform density distributions for the key geometric parameters to reduce bias. The simulations also provide redundant data in some ranges. Given the randomly sampled geometric and material properties, this redundancy improves the subsequent regression analysis as it captures the variability of the predictors (i.e., geometric and material parameters). The parametric simulation also complements gaps in experimental data as

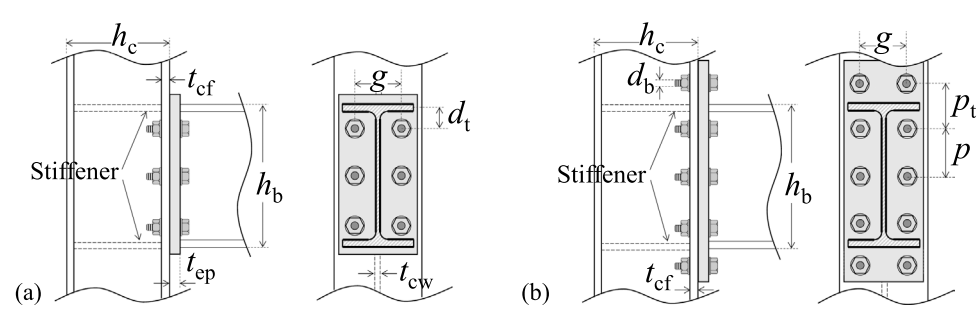


Fig. 1. Layout and definition of key geometric parameters for (a) FEPCs and (b) EEPCs.

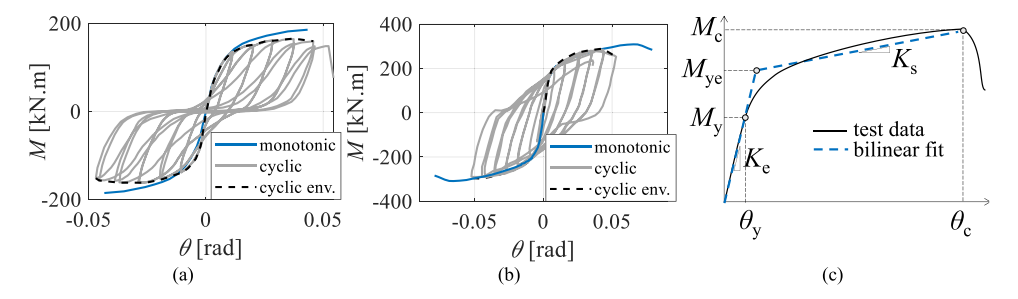


Fig. 3. Typical *M-θ* response under monotonic and cyclic load for: (a) FEPCs (b) EEPCs [test data from Shi et al. [22]]; and (c) deduced response parameters based on equal-area fitting [18].

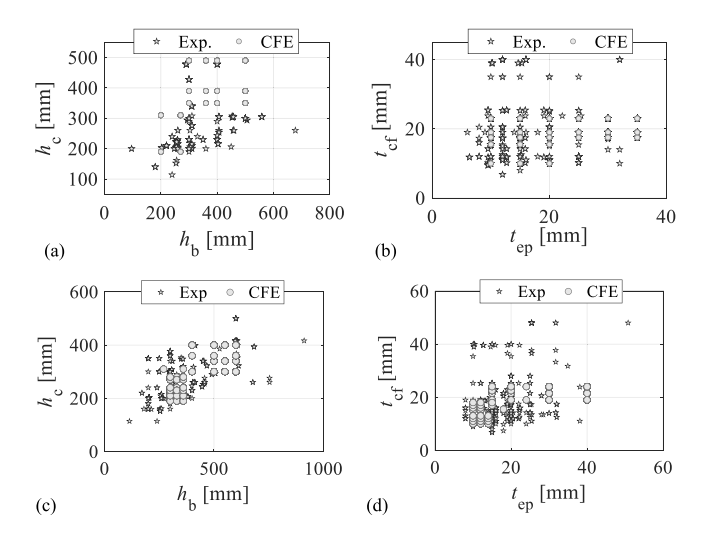


Fig. 4. Connection design space covered by the experimental and simulation datasets for: (a-b) FEPCs and (c-d) EEPCs.

demonstrated in Fig. 4, particularly the design space involving deeper columns ($h_c > 300$ mm) and thicker endplates ($t_{ep} > 20$ mm) for FEPCs, as well as deeper beams ($h_b > 400$ mm) for EEPCs.

The simulations involved full-scale exterior beam-to-column joints. In total, 2340 simulations were conducted: 920 for FEPC with a 4-bolt layout and 1420 for EEPC with an 8-bolt layout. The parametric ranges for the CFE simulations are summarized in Table 1. Permutations of these ranges were used to generate the parametric design space of the connections while randomly sampling the geometric parameters

Table 1
Summary of the design space covered by the CFE parametric simulations.

Type	#	Column	Beam	Bolt	$t_{ m ep}$	Material/Grade		
					[mm]	Bolt	Endplate	
FEPC	920	HEA 200;	IPE	M12;	10; 15;	8.8;	S275;	
		320; 360;	200;	M16;	20; 25;	10.9	S355	
		360; 400;	270;	M18;	30; 35			
		500	300;	M20;				
			360;	M22;				
			400;	M24;				
			500	M27;				
				M30				
EEPC	1420	HEA 200;	IPE	M18;	10; 12;	8.8;	S275;	
		220; 240;	300;	M20;	14; 15;	10.9	S355	
		280	330;	M24;	20; 30;			
		HEB 200;	360;	M30	40			
		220; 240;	400;					
		280; 300;	500;					
		340; 360;	550;					
		400	600					

^{*} beams and columns are fabricated from S355 grade steel

controlling the endplate geometry and the bolt layout (e.g., g, $d_{\rm b}$ and $p_{\rm t}$) from pre-defined normal distributions. All the generated connections satisfy the design limits for bolt spacing and edge distance. Additionally, geometric combinations that are not compatible (e.g., beam flange width is larger than that of the column) or those with highly disproportional component sizes that are not seen in design/construction practice were excluded (e.g., 30 mm endplate with M12 bolt). A list of the parametric simulation data and their geometric and material properties is provided as a supplementary electronic attachment to this paper.

The parametric simulations were conducted using the commercial software ABAQUS-FEA/CAE [26]. Fig. 5(a) shows the standard exterior joint layout, boundary conditions, and mesh. In all simulations, the column was 3 m long while the beam length was taken as four times the beam's depth. Both the column ends and the beam's free end were free to rotate (pinned) in the plane of the deformation. A monotonically increasing vertical displacement (Δ_v) is applied at the beam's free end up to bolt failure. All components were modelled using the modified quadratic tetrahedral C3D10M mesh elements. The mesh size was selected such that at least two mesh elements are used through a given component thickness. This resulted in a mesh size ranging from 5 to 15 mm. A nonlinear material model with kinematic hardening [27], based on the von Mises yield criteria, was employed. Young's modulus as well as the values of the yield and ultimate stresses and strains were randomly sampled from normal distributions representing the intrinsic variability of the respective material. The bolt head and nut were modelled using solid hexahedral elements (C3D8R) while an axial connector was used to model the bolt shank to reduce computational time. The connector is assigned a randomized trilinear force-elongation response dependent on the bolt's grade and geometric details, as prescribed in Ding and Elkady [28]. The beam-to-endplate and the stiffener-to-column (when present) welded connection is modeled with a tie constraint. A general hard contact interaction, with allowable separation after contact, was defined between the different moving parts. For the tangential behavior, a static friction coefficient equal to 0.35 is assumed. The explicit solver was used to trace the joint behavior up to bolt failure. Residual stresses in the hot-rolled column and beam sections are not modelled as they would not have a notable effect on the connection response [29,30]. Geometric imperfections were not considered in the endplate or the beam. The latter is not critical when dealing with partial-strength connections where only limited beam yielding is expected to occur but no beam local buckling. The CFE modeling approach was thoroughly validated against several joints with various configurations. Fig. 5(b-c) show a couple of those validations in the form of comparisons between test and simulation moment-rotation data. More validations can be found in the paper's supplementary material.

Table 2 summarizes the statistical parameters of the main geometric and material parameters of the regression dataset. The dataset covers joints with shallow 100 mm beams up to deep 754 mm beams. Endplates as thin as 6 mm thick and as thick as 50 mm are included as well as M12 to M36 bolts. The materials ranged from low-carbon S235 (A36) to high-

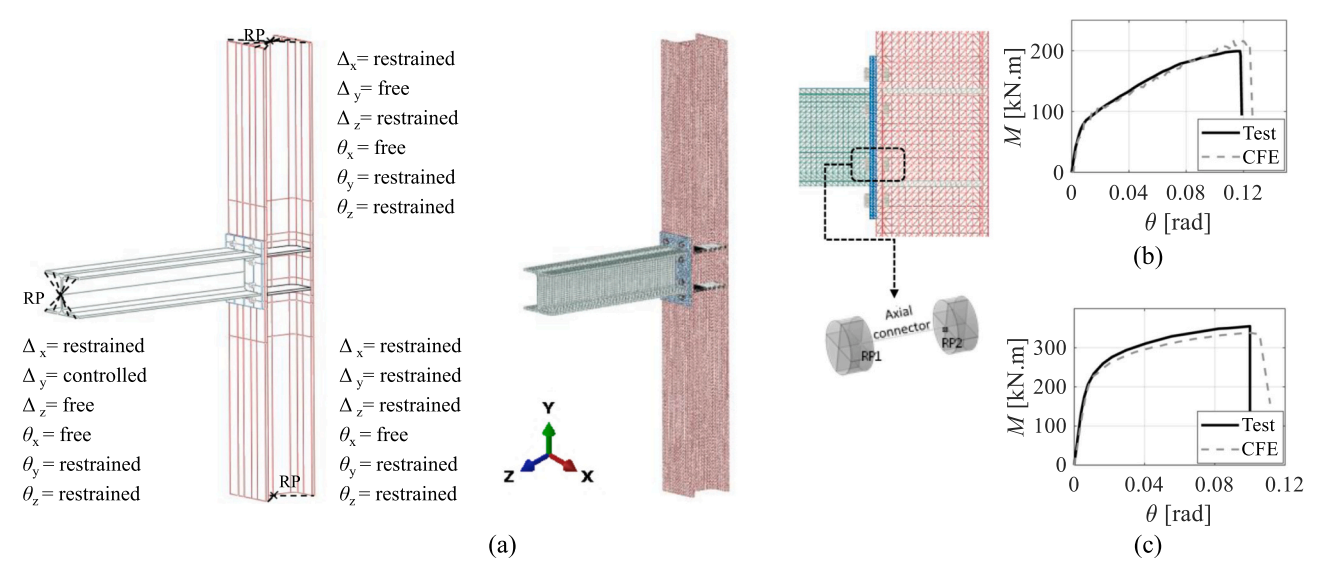


Fig. 5. (a) Standard features of the analyzed CFE joints and sample validations of the CFE modeling approach against test data for joints with (b) FEPC [test data by Rölle [31]] and (c) EEPC [test data by Augusto et al. [32]].

 $\begin{tabular}{ll} \textbf{Table 2} \\ \textbf{Statistical summary of the features within the regression datasets [units: mm and MPa].} \\ \end{tabular}$

	FEPC				EEPC				
Parameter	μ	σ	min	max	μ	σ	min	max	
$h_{\rm c}$	340	88	114	490	313	70	114	500	
$h_{ m b}$	394	115	96	678	472	122	114	754	
$t_{ m ep}$	17	7	6	35	21	9.7	8	50	
$d_{ m b}$	21	5	12	30	24	5	16	36	
g	114	21	50	230	118	15	60	190	
d_{t}	53	18	24	118	-	-	-	-	
p_{t}	-	-	-	-	136	23	62	205	
$f_{ m y,P}$	355	82	214	1045	352	63	214	1022	
$f_{\rm y,C}$	374	48	243	717	389	47	220	1017	
$f_{ m y,b}$	846	141	570	1200	921	134	574	1217	

 μ : mean σ : standard deviation

strength S960 steel. A wide statistical distribution is also observed for the characteristic geometrical parameters g, $d_{\rm t}$, and $p_{\rm t}$ that describe the bolt layout at the beam's tension flange.

3. Target response parameters and predictors

Referring to Fig. 3(c), a bilinear backbone curve is used to represent the connection's M- θ response. While nonlinear mathematical models, such as the Menegotto-Pinto [33] and Richard-Abbott [34] models, are better at capturing the smooth transition between the elastic and plastic branches; they fail to account for in-cycle and cyclic strength/stiffness degradation mechanisms, which are crucial for earthquake simulation. In contrast, the bilinear backbone curve can be easily integrated with existing multilinear phenomenological cyclic degradation models, such as the IMK models [35], which are commonly used in system-level simulations of steel components [3,7,9].

Four parameters are required to construct the backbone curve. Those are the elastic rotation stiffness (K_e), the effective yield (plastic) moment (M_{ye}), the capping moment (M_c), and the capping rotation (θ_c). Additionally, the yield moment (M_y) is also considered. Although M_y does not affect the definition of the backbone curve, it represents a key limit state that is needed to define acceptance criteria and fragility functions as part of performance-based structural evaluations [36,37]. It is important to note that the moment represents the moment measured at the column face and the rotation represents the total joint rotation, excluding the

elastic rotations of the column and the beam members. Details of the fitting procedure used to deduce the response parameters can be found in Elkady [18].

Several geometric and material parameters control the response of partial-strength endplate connections (i.e., response predictors). To simplify the model, the predictors that most influence the behavior are selected based on the connections' deformation mechanics demonstrated in Fig. 2, which are corroborated by an evaluation of the response-predictor correlations. For both connection types, those include the beam and column depths, the thickness of the endplate, column web, and column flange, the bolt diameter, the bolt gauge length, and the yield and ultimate stress values for the different connection components. Additionally, the characteristic geometric parameters $d_{\rm t}$ and $p_{\rm t}$ that control the endplate bending deformation in FEPCs and EEPCs, respectively, are considered. The dependency of the response parameters on the selected predictors is well-established in the literature [14,24,38–40].

4. Regression model

The multivariate power expression, given by Eq. (1), is used to develop the empirical equations for the different backbone response parameters, where Y is the dependent variable (response parameter), X_i is the i-th independent variable (geometric/material predictor), β_i is the coefficient/exponent for the i-th predictor, n is the number of predictors, and ε is the model error. This form of regression equations is widely used in the literature as part of structural modeling guidelines and standards [3,5,7]. This form allows for conducting linear regression in the log-log space while capturing nonlinear correlations in the original space. This model is also popular for its simple form and the ability to infer correlations between the dependent and independent variables from the equation exponents.

$$Y = \beta_0 \cdot \prod_{i=1}^n X_i^{\beta_i} + \varepsilon \tag{1}$$

Multivariate linear regression is conducted using the logarithmic values of the response parameters and the predictors. A linear relationship is thus assumed between the dependent and the independent variables in the log-log space. Least-squares fit is used to regress the data and obtain the model coefficients. It is worth noting that in the regression procedures, a larger weight (proportional to the simulation-to-experimental dataset size ratio) is assigned to the experimental

dataset. The larger weight is meant to reflect the confidence in the experimental data and their ability to capture real joint conditions. To check for multicollinearity, the Variance Inflation Factor (VIF) scores were quantified. As a rule of thumb, any feature achieving a VIF score larger than 5.0 was removed from the model to help reduce the model size and eliminate redundancy [41]. The model for each response parameter was also checked for overfitting through a bias-variance analysis by consistently dividing the data into a training, testing, and validation subsets (with a 70 %-10 %-20 % split, respectively) and ensuring that the performance fit metrics are consistent across subsets. For the final models, the entire dataset was used for inference (i.e., regression coefficient estimation). Finally, it is worth noting that conducting regression using scaled/dimensionless predictor values was also examined, and no notable difference was observed in the model performance compared to using the absolute values. The latter approach was consequently selected given its simpler and direct mathematical form.

To improve the regression and the model accuracy, the regression equation for each response parameter of a given connection type is separated based on the presence or absence of column flange stiffeners (noted henceforth as the *stiffened* and *unstiffened* cases, respectively). Furthermore, the joint types (noted henceforth as the external joints/interior ones with asymmetric beam loading and internal joints with symmetric beam loading) are herein used to separate the regression equations for the elastic stiffness. This is mainly because the panel zone shear behavior is highly controlled by the presence of stiffeners and loading directions. Specifically, under symmetric loading (i.e., joints under equal but opposing bending moments, as in the case of gravity load or column loss scenarios), the panel zone's shear distortion is restrained while under asymmetric loading (i.e., joints under equal/unequal and co-directional moments, as in the case of lateral loads), the panel zone's shear distortion is amplified.

The model performance is quantitatively assessed by several metrics: the coefficient of determination (R^2) , and the percentage of data falling within an error ratio (predicted to measured ratio) of ± 20 % (P_{20}) and ± 50 % (P_{50}) . The 20 % error limit is commonly used in the literature as an upper bound for assessing acceptable predictions. The 50 % error limit is used to demonstrate that the developed models do not produce largely erroneous estimates. To quantify the variability in the model prediction, the standard deviation of the residual error (σ_{ϵ}) is reported. The σ_{ϵ} , which is closely related to the root mean square error (*RMSE*), is expressed in the same units of the predicted response parameter. The regression metrics are summarized in Table 3 for all the developed

regression equations, including the mean and standard deviation of the absolute relative error ($\mu_{[e,rel]}$ and $\sigma_{[e,rel]}$, respectively) to assist with probabilistic simulations. In general, all regression equations achieve a high R^2 score larger than 0.85. For the strength parameters (M_y , M_{ye} , and M_c/M_{ye}), the model predicts more than 70 % of the data points with an error of less than ± 20 %. For all other models, the prediction error does not exceed ± 50 %, excluding a few cases for sensitive K_e and θ_c parameters that experience large variability.

Qualitatively, the model performance is visualized in Fig. 6, which shows the response parameter histogram, the predicted versus measured values, and the histogram of the residual error (predicted minus measured value) for the unstiffened EEPC models. Similar plots can be observed for the stiffened case as well as FEPCs but are not shown here for brevity. The figure demonstrates a good match between the predicted and measured values of the regression dataset, where the scatter is close to the 1:1 reference line. This was already expected from the high P_{20} values in Table 3. Larger scatter variability is observed for the $K_{\rm e}$ and $\theta_{\rm c}$ parameters. These are intrinsically sensitive parameters as discussed in detail in the following sections. The spread of both the experimental and simulation datasets (differentiated by different markers in the scatter plots), about the 1:1 reference line, is consistent, which further confirms the soundness of the latter.

The regression quality is further checked against the Gauss-Markov theory conditions set in Chatterjee and Hadi [42]. In particular, the residual error has a mean value close to zero and is normally distributed for all response parameters. This can be inferred from the error histograms and in the sample quantile-quantile (QQ) plot shown in Fig. 7(a) for the M_{ve} parameter. Quantitatively, the normality of the residual error (null hypothesis) was confirmed by calculating the p-value based on the Lilliefors test [43]. The error distribution also satisfies the homoscedasticity assumption, where an even error variance is observed with respect to the predicted values. This can be visually inspected in Fig. 7 (b) and was confirmed by the Breusch-Pagan test [44]. Accordingly, the reported σ_{ϵ} can be used in support of probabilistic simulations, structural reliability assessment, and the investigation of modeling uncertainty effects. Additionally, the mean and standard deviation of the absolute relative error (i.e., residual error divided by predicted value, $\varepsilon_{\rm rel}$) are reported in Table 3. Note that $\mu_{|\varepsilon,rel|}$ does not exceed 20 % of the predicted value for all modes. This scale-invariant performance metric can also be used to quantify uncertainty.

Table 3Summary of performance metrics for the proposed regression equations.

							FEPC						
	Uns	stiffened					S	tiffened					
	$K_{\rm e}$		$M_{ m y}$	М	ye	θ_{c}	K	-e	$M_{ m y}$	M_{y}	re	θ_{c}	
R^2	0.9	0	0.95	0.	94	0.86	0	.93	0.94	0.9	92	0.95	
P_{20}	0.6	3	0.67	0.	71	0.40	0	.65	0.69	0.7	73	0.58	
P_{50}	0.9	6	1.00	0.	99	0.83	0	.96	1.00	1.0	00	0.97	
$\sigma_{arepsilon}$	831	10	22	33	3	0.015	8	227	20	31		0.012	
$\mu_{ \varepsilon,rel }$	0.1	9	0.17	0.	14	0.20	0	.17	0.18	0.1	13	0.18	
$\sigma_{ \varepsilon,rel }$	0.1	6	0.13	0.	10	0.17	0	.13	0.13	0.1	1	0.13	
191						EI	EPC						
	Unstiffened	Unstiffened					Stiffened						
	K _e		$M_{ m y}$	$M_{ m ye}$	$ heta_{ m c}$	$\frac{M_{\rm c}}{M_{\rm ye}}$	K _e		$M_{ m y}$	$M_{ m ye}$	$ heta_{ m c}$	$\frac{M_{\rm c}}{M_{\rm ye}}$	
	Asym.	Sym.				,-	Asym.	Sym.				,-	
R^2	0.96	0.87	0.96	0.97	0.94	0.47	0.95	0.95	0.96	0.96	0.92	0.53	
P_{20}	0.97	0.85	0.78	0.85	0.64	0.98	0.87	0.94	0.71	0.80	0.63	0.98	
P_{50}	0.98	0.95	1.00	1.00	1.00	1.00	0.97	0.97	1.00	1.00	1.00	1.00	
$\sigma_{?}$	7955	9949	46	50	0.007	0.12	10518	11354	52	58	0.009	0.11	
$\mu_{ ?,rel }$	0.11	0.13	0.13	0.11	0.18	0.07	0.18	0.08	0.14	0.12	0.17	0.06	
$\sigma_{ ?,rel }$	0.08	0.12	0.09	0.09	0.11	0.06	0.13	0.12	0.09	0.09	0.11	0.06	

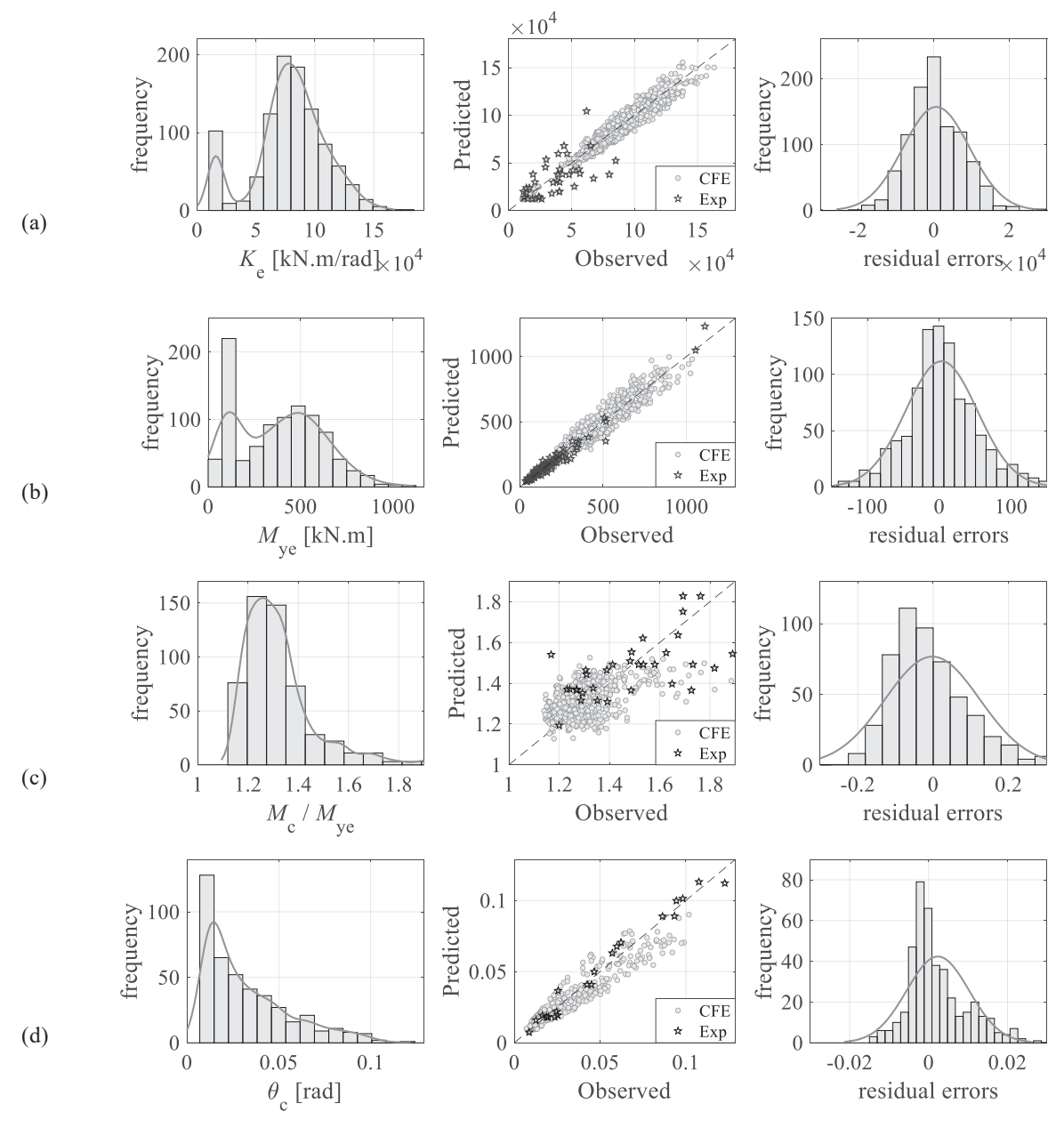


Fig. 6. Response parameter histogram and regression model performance for unstiffened EEPC: (a) K_e (asym.), (b) M_{ye} , (b) M_c/M_{ye} , and (d) θ_c .

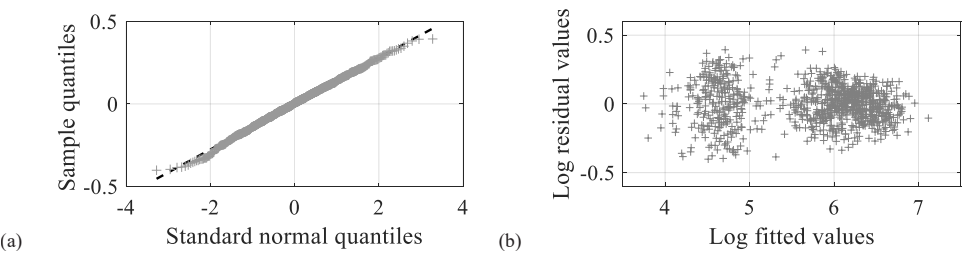


Fig. 7. Statistical analysis plots of the residual error for the unstiffened EEPCs M_{ve} regression model: a) QQ plot, and b) residual error versus predicted values.

5. Proposed regression equations

The regression equations are presented in this section. The predictors in those equations are defined in mm and MPa units while the output stiffness, strength, and rotation values are in kN.m/rad, kN.m, and radians, respectively.

5.1. Elastic rotational stiffness

The elastic rotation stiffness (K_e) regression equations for FEPCs and

an elastic rotational stiffness that ranges between 0.79 and 17.8 $E_b I_{x,b}/L_b$ with a median value of 5.0, where E_b , $I_{x,b}$, and L_b are the beam's Young's modulus, moment-of-inertia about the strong axis, and length (a constant length equal to 15 times the beam height is assumed). Further assessment of FEPCs' stiffness rigidity can be found elsewhere [18]. EEPCs can achieve between 2.0 and 55 $E_b I_{x,b}/L_b$ with a median value of 6.4. Accordingly, both FEPCs and EEPCs sit comfortably within the semi-rigid classification range as per both AISC [48] and Eurocode 3 [49], although the latter can also develop high stiffness within the fully rigid range.

$$K_{\rm e}({\rm FEPC}) = \begin{cases} 3.4 {\rm x} 10^{-1} & d_{\rm t}^{-0.387} & g^{-1.457} & t_{\rm ep}^{0.874} & t_{\rm cf}^{-0.564} & t_{\rm cw}^{1.168} & d_{\rm b}^{0.393} & h_{\rm b}^{2.545} & h_{\rm c}^{0.023} & {\rm stiffened} \\ 5.2 {\rm x} 10^{-3} & d_{\rm t}^{-0.617} & g^{-0.319} & t_{\rm ep}^{0.634} & t_{\rm cf}^{0.108} & t_{\rm cw}^{-0.156} & d_{\rm b}^{0.977} & h_{\rm b}^{2.274} & h_{\rm c}^{0.236} & {\rm unstiffened} \end{cases}$$
 (2)

$$K_{\rm e}({\rm EEPC}) = \begin{cases} 4.6 {\rm x} 10^{-1} & p_{\rm t}^{-1.60} & g^{-0.646} & t_{\rm ep}^{0.514} & t_{\rm cf}^{0.360} & t_{\rm cw}^{-0.28} & d_{\rm b}^{0.40} & h_{\rm b}^{1.97} & h_{\rm c}^{1.280} {\rm stiffened; asym} \\ 5.9 & p_{\rm t}^{-1.21} & g^{-0.453} & t_{\rm ep}^{1.40} & t_{\rm cf}^{4.380} & t_{\rm cw}^{-4.15} & d_{\rm b}^{0.56} & h_{\rm b}^{2.15} & h_{\rm c}^{-0.55} {\rm stiffened; sym} \end{cases} \\ 1.4 {\rm x} 10^{-3} & p_{\rm t}^{0.170} & g^{-0.460} & t_{\rm ep}^{0.413} & t_{\rm cf}^{-0.44} & t_{\rm cw}^{0.340} & d_{\rm b}^{0.21} & h_{\rm b}^{1.47} & h_{\rm c}^{1.470} {\rm unstiffened; asym} \\ 3.0 {\rm x} 10^{-3} & p_{\rm t}^{0.170} & g^{-0.720} & t_{\rm ep}^{0.430} & t_{\rm cp}^{0.470} & t_{\rm cw}^{1.040} & d_{\rm b}^{1.08} & h_{\rm b}^{1.64} & h_{\rm c}^{0.230} {\rm unstiffened; sym} \end{cases}$$

EEPCs are given by Eqs. (2) and (3), respectively. The elastic stiffness is a sensitive parameter that is affected by the geometry of all components and bolt layout parameters. To maintain a practical form of the equation, only eight geometric parameters were selected that are deemed the most influential in controlling the bolt elastic elongation, the column web deformation in shear, and the bending of the endplate and column flange. The negative exponents demonstrate the expected negative correlation between $K_{\rm e}$ and both $d_{\rm t}$ and $p_{\rm t}$ parameters for FEPCs and stiffened EEPCs, respectively, while the positive exponents demonstrate the positive correlation with $t_{\rm ep}$ and $h_{\rm b}$. In the stiffened FEPCs, the column depth becomes less influential on $K_{\rm e}$, as implied by the lower exponent values. Nonetheless, the column parameters are kept in the equations to maintain consistency.

The K_e equations have a satisfactory performance (refer to Table 3). However, K_e prediction errors larger than 50 % may be observed. Notwithstanding the regression error, part of this uncertainty cannot be alleviated as it is related to a) the K_e deduction method, which accounts for about 20 % uncertainty in the measured K_e values [18], and b) the effect of plate imperfection and bolt preload level on the level-of-fit between the joined components, which can account for about 50 % difference [45–47]. These effects are evident in the experimental dataset

5.2. Yield moment

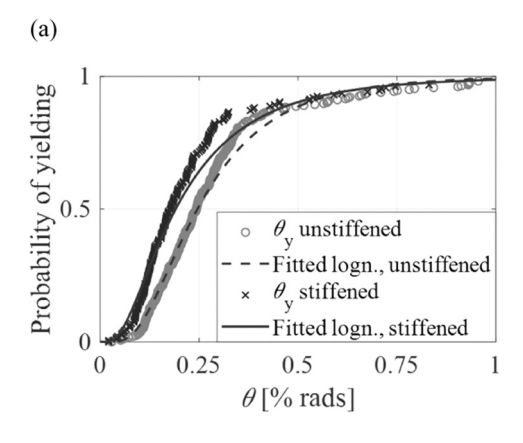
The moment at the onset of yielding in any of the connection components is predicted by Eqs. (4) and (5) for FEPCs and EEPCs, respectively. The equations incorporate six geometric parameters and two material parameters. For the latter, the yield stress of the endplate $(f_{v,P})$ and the column $(f_{y,C})$ are used. Those are the components that commonly experience plastic deformations in these types of connections. The column web panel's geometric parameters and the bolt's material properties are not considered, as they do not improve the model performance and develop a high VIF score. Plus, these components only control the onset of yielding in rare cases, e.g., when thick plates are employed with either a small size (weaker) bolt or column. Referring to Fig. 6(b) and Table 3, the proposed equations have a high performance, with a P_{20} larger than 0.7. Additional constraints shall be applied to these equations. Specifically, for FEPC, $M_{\rm v}$ shall be between 38 % and 80 % of $M_{\rm ve}$ while for EEPCs, the value shall be within 44 % and 84 % of $M_{\rm ve}$.

$$M_y \quad (\text{FEPC}) = \left\{ \begin{array}{llll} 1.06 \text{x} 10^{-7} & d_{\text{t}}^{0.269} & g^{-0.414} & t_{\text{ep}}^{1.156} & t_{\text{cf}}^{0.324} & d_{\text{b}}^{0.278} & h_{\text{b}}^{1.479} & f_{\text{y,P}}^{0.750} & f_{\text{y,C}}^{0.516} & \text{stiffened} \\ 5.04 \text{x} 10^{-9} & d_{\text{t}}^{-0.11} & g^{-0.613} & t_{\text{ep}}^{1.013} & t_{\text{cf}}^{0.328} & d_{\text{b}}^{0.397} & h_{\text{b}}^{2.069} & f_{\text{y,P}}^{0.884} & f_{\text{y,C}}^{0.784} & \text{unstiffened} \end{array} \right.$$

and not the simulation one, which involved perfect geometry (refer to the scatter in Fig. 6(a)).

By evaluating the regression dataset, it is noted that FEPCs develop

0.38
$$M_{ye} \le M_y \le 0.80$$
 M_{ye} (4)



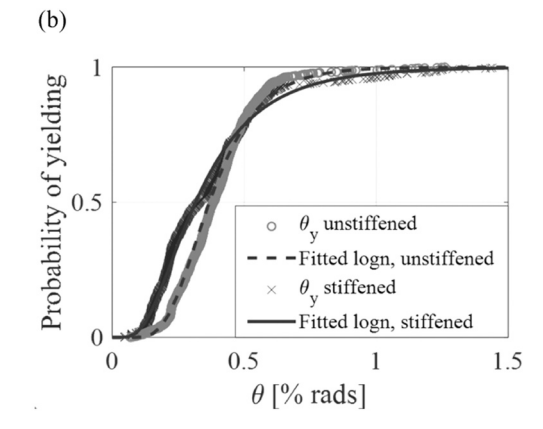


Fig. 8. Fragility curves for the yielding limit state for (a) FEPCs and (b) EEPCs.

Table 4
Statistical parameters of the lognormal fragility curves for the yielding limit state.

Connection type	Column flange	$\mu_{ heta y}$	$\mu_{ ext{ln } heta ext{y}}$	$\sigma_{ m ln~ heta y}$
FEPC	unstiffened	0.30 % rads	-1.404	0.589
	stiffened	0.28 % rads	-1.658	0.742
EEPC	unstiffened	0.40 % rads	-5.600	0.390
	stiffened	0.37 % rads	-5.760	0.580

lognormal distribution (i.e., the mean and standard deviation of the logarithmic θ_y values) are summarized in Table 4. For both connection types, yielding occurs around 0.35 % rads on average. At 1 % rotation, the probability of reaching the yielding limit state is almost 100 %.

5.3. Effective yield moment

The effective yield moment corresponds to the full plasticization of one of the connection's components and the initiation of the post-yield hardening phase. Using the same predictors as the yield moment, M_{ye} for FEPCs and EEPCs is given by Eqs. (6) and (7), respectively. Like M_y , the

$$M_{\rm y} \quad ({\rm EEPC}) = \left\{ \begin{array}{ccccccccc} 3.78 \times 10^{-7} & p_{\rm t}^{-0.37} & g^{0.420} & t_{\rm ep}^{0.80} & t_{\rm cf}^{0.144} & d_{\rm b}^{1.12} & h_{\rm b}^{1.47} & f_{\rm y,P}^{0.91} & f_{\rm y,C}^{-0.11} & {\rm stiffened} \\ 6.80 \times 10^{-6} & p_{\rm t}^{-0.36} & g^{-0.72} & t_{\rm ep}^{0.72} & t_{\rm cf}^{0.440} & d_{\rm b}^{0.88} & h_{\rm b}^{1.73} & f_{\rm y,P}^{0.61} & f_{\rm y,C}^{0.32} & {\rm unstiffened} \end{array} \right.$$

0.44
$$M_{ye} \le M_y \le 0.84 M_{ye}$$
 (5)

Supplementary to the M_y equations, Fig. 8 shows the empirical cumulative distribution functions (CDFs) for the yield rotation (θ_y) along with fitted lognormal CDFs. Those are essentially the fragility curves for the yielding limit state. The statistical parameters for the fitted

 $M_{\rm ye}$ equations have high-performance metrics. FEPCs are expected to develop $M_{\rm ye}$ that is between 5 % and 77 % of the connected beam plastic moment $M_{\rm p,b}$. EEPCs can develop a larger 17–108 % of $M_{\rm p,b}$. Note that for EEPCs, $M_{\rm ye}$ can approach or slightly exceed $M_{\rm p,b}$. This takes place when a balanced design is achieved where the connection components (mainly the endplate) plastically deform simultaneously with the onset of beam flange yielding/buckling.

$$M_{ye} \quad (FEPC) = \begin{cases} 1.97 \times 10^{-5} & d_{t}^{0.090} & g^{-0.30} & t_{ep}^{0.674} & t_{cf}^{0.414} & d_{b}^{1.223} & h_{b}^{1.053} & f_{y,P}^{0.419} & f_{y,C}^{0.196} & stiffened \\ 6.87 \times 10^{-6} & d_{t}^{-0.33} & g^{0.534} & t_{ep}^{0.620} & t_{cf}^{0.138} & d_{b}^{1.187} & h_{b}^{1.699} & f_{y,P}^{0.629} & f_{y,C}^{0.161} & unstiffened \end{cases}$$
(6)

$$M_{ye} \quad (EEPC) = \begin{cases} 6.30 \times 10^{-5} & p_{t}^{-0.650} & g^{0.090} & t_{ep}^{0.59} & t_{cf}^{0.28} & d_{b}^{1.29} & h_{b}^{1.350} & f_{y,P}^{0.61} & f_{y,C}^{-0.04} & \text{stiffened} \\ 3.70 \times 10^{-5} & p_{t}^{-0.136} & g^{-0.51} & t_{ep}^{0.56} & t_{cf}^{0.56} & d_{b}^{0.95} & h_{b}^{1.350} & f_{y,P}^{0.35} & f_{y,C}^{0.350} & \text{unstiffened} \end{cases}$$

$$(7)$$

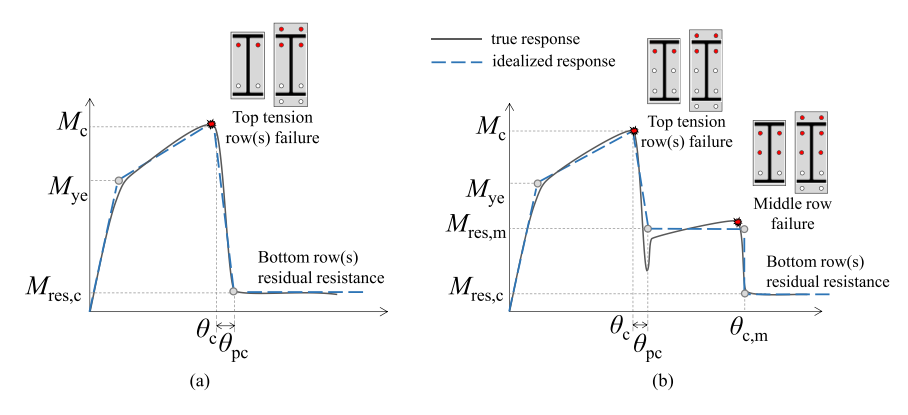


Fig. 9. Idealized monotonic backbone parameters in the post-capping range of connection: (a) without middle bolt row, and (b) with middle bolt row.

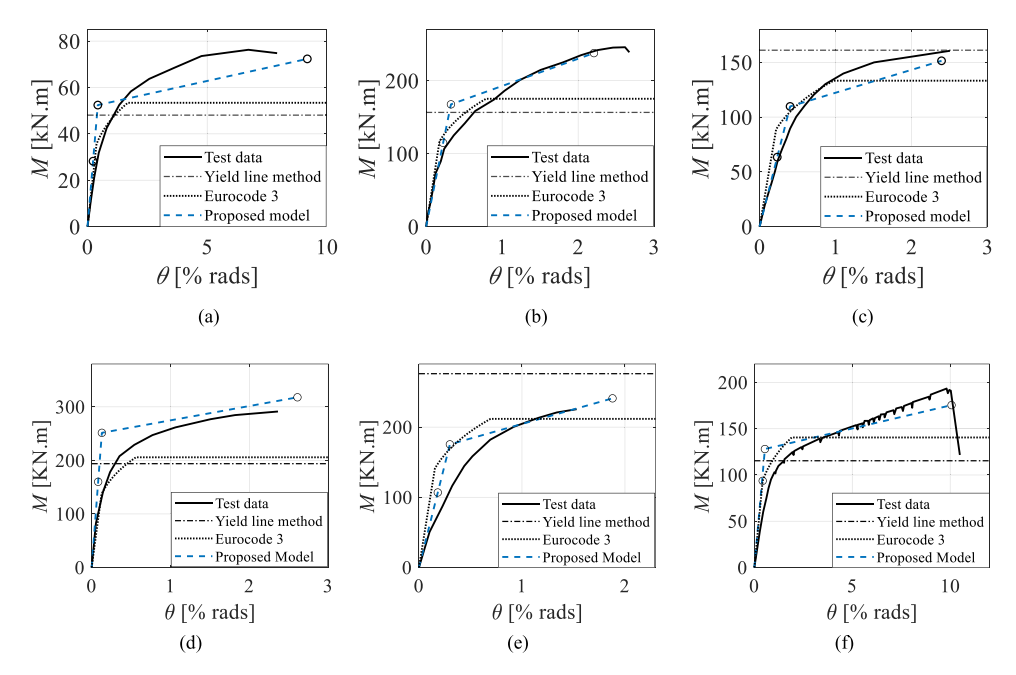


Fig. 10. Comparisons of the proposed backbone model, the yield line method, and the Eurocode 3 component method with representative test data: (a) unstiffened FEPC [test data by Ostrander [52]]; (b) unstiffened FEPC [test data by Rölle [31]]; (c) stiffened FEPC [test data by Jenkins et al. [53]]; (d) stiffened EEPC [test data by Sherbourne [54]]; (e) stiffened EEPC [test data by Prinz et al. [56]].

Table 5Summary of predicited-to-measured ratios for representative test specimens.

		Yield line	Eurocode 3		Proposed n			
		M _{ye} 0.88	K _e	$M_{ m ye}$	K _e	$M_{ m ye}$	$M_{\rm c}$	θ_{c}
FEPC	Unstiffened interior sym. [52]		0.97	0.97	1.40	0.95	0.97	1.18
	Unstiffened interior sym. [31]	1.03	1.01	1.16	0.78	1.10	0.97	0.85
	Stiffened interior sym. [53]	1.29	1.64	1.07	1.09	0.88	0.94	0.96
EEPC	Stiffened interior sym. [54]	0.87	1.19	0.92	1.23	1.12	1.11	1.08
	Stiffened interior sym. [55]	1.80	1.98	1.39	1.15	1.14	1.08	1.20
	Unstiffened exterior [56]	1.03	1.48	1.25	1.40	1.14	0.95	1.02

5.4. Post-yield strength ratio

To define the connections' capping (ultimate) moment, the post-yield strength ratio $(M_{\rm c}/M_{\rm ye})$ is used. Traditionally, this parameter is stable and does not experience much variability between different connection layouts and material properties. Therefore, it is recommended for defining the post-yield increase in strength (i.e., strain hardening) compared to the post-yield stiffness $K_{\rm S}$ [3,7]. Utilizing the

ratio $M_{\rm c}/M_{\rm ye}$ also resulted in a better model compared to predicting $M_{\rm c}$ directly. For EEPCs, $M_{\rm c}/M_{\rm ye}$ can be computed using Eq. (8), with a lower limit of 1.05 $M_{\rm ye}$ and an upper limit of 1.7 $M_{\rm ye}$. The equation uses similar predictors as the moment equation with the addition of the material ultimate stress values to capture the level of material strain hardening of the different connection components before failure.

In the case of the FEPCs, the same set of predictors was not able to produce a reasonable model, as a very low R^2 was observed (< 0.25) along with a high P_{20} value larger than 0.9. This implies that the predictors do not account for much of the variation in the dependent

variable. Accordingly, the statistical parameters (mean and standard deviation) of $M_{\rm c}/M_{\rm ye}$ can be directly used in this case to sample the distribution. Those can be taken as 1.37 and 0.16, respectively.

5.6. Post-capping response

The bilinear model presented earlier is sufficient for design purposes. For numerical simulations, however, a sudden drop in strength (to zero)

$$1.05 \le \frac{M_{\rm c}}{M_{\rm ve}} \le 1.7 \tag{8}$$

5.5. Ultimate/capping rotation

The capping point is defined using the $M_{\rm c}/M_{\rm ye}$ ratio and the value of the rotation at the capping strength ($\theta_{\rm c}$). Note that the capping point is coincident with failure in the case of partial-strength endplate connections since failure is associated herein with bolt tensile rupture. In other words, the post-capping (negative) slope can be ignored, and a sudden drop in strength can be assumed. The capping rotation can be predicted using Eqs. (9) and (10) for FEPCs and EEPCs, respectively. The equations use similar predictors as the previous ones, with the inclusion of the ultimate stress of the bolt material ($f_{\rm u,b}$). The observed failure rotation in both connection types is around 3.8 % rads on average. EEPCs can possess comparable ductility to that of the more flexible FEPCs. Both connections can reach up to 12 % rads. Unstiffened connections develop around 20 % larger ductility compared to stiffened ones. This is, however, dependent on the governing deformation mode.

without a reasonable negative post-capping stiffness may lead to numerical instabilities once a given connection fails in a frame model. Consequently, failure progression through the frame model will not be quantifiable. For that reason, further guidelines are provided in this section for the modeling of the post-capping portion of the backbone curve. Given that laboratory tests stop as soon as first bolt failure takes place, the guidelines developed henceforth are based solely on the CFE simulations where the entire backbone curve (damage progression) can be traced.

For 4-bolt FEPCs and 8-bolt EEPCs (see Fig. 9(a)), following the failure of the top -tension- bolt row(s), the connection resistance reverts to $M_{\rm res,c}$ which is the residual moment resistance sustained by the bottom -compression- bolt row(s). In average, $M_{\rm res,c}$ is 10 % and 20 % of $M_{\rm c}$ for FEPCs and EEPCs, respectively, with a coefficient of variation (COV) of 0.42 for both connections. The corresponding post-capping rotation ($\theta_{\rm pc}$) is 0.5 % rads on average with a COV of 0.44. Note here that $M_{\rm res,c}$ can be sustained to exceedingly large rotations. For practical purposes, the ultimate rotation ($\theta_{\rm u}$) at which the resistance reaches zero can be taken equal to 20 % rads.

For 6-bolt FEPCs and 10-bolt EEPCs (i.e., with a middle bolt row as shown in Fig. 9(b)), following the failure of the top -tension- bolt row(s), the connection resistance reverts to $M_{\rm res,m}$ which is the moment resis-

$$\theta_{\rm c} \ge 1.3 \frac{M_{\rm ye}}{K_{\rm e}} \tag{9}$$

tance sustained by the middle and bottom bolt row(s). $M_{\rm res,m}$ can be estimated based on the expressions given in Eq. (11). The $M_{\rm res,m}$ value corresponds roughly to about 55–65 % of $M_{\rm max}$ for the cases of FEPCs and EEPCs, respectively. The middle bolt row will fail at a total rotation ($\theta_{\rm c,m}$) that is about two times $\theta_{\rm c}$. Eventually, the connection reverts to $M_{\rm res,c}$ as previously discussed.

$$\theta_{c} \quad (\text{EEPC}) = \begin{cases} 9.6 \text{x} 10^{-5} & p_{t}^{0.840} & g^{-1.10} & t_{ep}^{-0.300} & t_{cf}^{-1.34} d_{b}^{3.90} h_{b}^{-0.91} f_{y,P}^{-0.71} f_{y,C}^{-0.71} f_{y,C}^{1.5} \\ 2.7 \text{x} 10^{-2} & p_{t}^{-0.27} & g^{0.740} & t_{ep}^{-0.205} & t_{cf}^{-1.40} d_{b}^{3.77} h_{b}^{-1.20} f_{y,P}^{-0.33} f_{y,C}^{-1.21} f_{u,b}^{1.10} & \text{unstiffened} \end{cases}$$

$$\theta_{\rm c} \geq 1.5 \frac{M_{\rm ye}}{K_{\rm e}} \tag{10} \qquad M_{\rm res,m} = \begin{cases} \frac{d_{\rm t}}{h_{\rm b}/2} & {\rm FEPC(COV} = 0.11) \\ \\ \frac{h_{\rm b} - p}{h_{\rm b}} & {\rm EEPC(COV} = 0.08) \end{cases} \tag{11} \label{eq:mesmap}$$

6. Model demonstration

To visually demonstrate and validate the proposed model, the predicted backbone curves are plotted in Fig. 10 against the data from several representative test specimens from the literature that failed by bolt rupture. Markers are used to highlight the main backbone points including the onset of yielding. In the same plots, the code-based predictions based on the yield line method [13,14,50] and the mechanical component-based method of Eurocode 3 [51], are superimposed for reference. Quantitively, the ratios of the predicted response parameters to the measured ones are summarized in Table 5. In general, the model reasonably captures the moment-rotation response with good prediction of the critical K_e and M_{ve} quantities. The post-yield slope and the failure points, which are not addressed by the other two models, are also well predicted across different connection layouts and material properties. The observed \pm divergence from the true behavior is a common byproduct of the data fitting process which minimizes the global error. Referring to Table 5, this divergence (error ratios), with respect to any response parameter, falls within the acceptable error range described and explained earlier in 6. Notably, this model uncertainty can be addressed by considering either the lower or upper bounds for the backbone response, depending on the purpose. Those can be defined using the tabulated residual error metric, as discussed earlier.

7. Model limitations and practical implementation

7.1. General applicability

The proposed models are limited to partial-strength endplate connections where the connection's plastic strength is less than that of the connected beam. The model applicability is valid as long as the geometric and material parameters of the connection are within the ranges of the employed dataset. Nonetheless, given that the regression models capture the underlying effects of the different geometric/material features on the response parameters, the model could be used in concept-with caution- to extrapolate beyond its range of applicability. The model validity extends to FEPCs with more than two bolt rows (i.e., 4-bolt layout) and EEPCs with more than four bolt rows (i.e., 8-bolt layout). Connections with different layouts are already part of the experimental database. Additionally, interior bolt rows are generally used to carry shear forces and do not have direct impact on the connection stiffness or strength.

7.2. Model limitations

The models predict the connection ductility considering the bolt rupture as the sole failure mode. This assumes that weld failure does not occur prior to bolt failure. Considering proper weld design and fabrication, this assumption is valid for FEPCs in general and for EEPCs that do not develop large moment capacity (less than 0.7 $M_{\rm p,b}$). For larger capacity EEPCs involving deep beams ($h_{\rm b} >$ 400) and stiff endplates ($p_{\rm t}/t_{\rm ep} <$ 9), the larger strains induced near the weld may result in early failure. Such failure mode and others such as bolt stripping or plate tearing need to be assessed separately, perhaps using probabilistic fragility models. Additionally, under cyclic drifts, failure may occur earlier due to ultra-low-cycle fatigue. This issue requires further investigation.

The post-failure response is deduced here based only on CFE simulations, due to absence of experimental data at very large deformations. Although, the CFE modeling approach is thoroughly validated, it is only validated up to -first- failure. Therefore, it would be beneficial to have future experimental data that explores the post-failure response.

7.3. Model implementation

The models can be used to define either the monotonic backbone or

cyclic envelope curve as part of existing phenomenological hysteretic component models [35]. In the case of seismic simulation, the hysteretic response parameters will need to be calibrated, specifically the parameters that control the level of pinching. In the presence of a concrete slab that is working compositely with the steel beam, the backbone parameters will need to be modified to reflect the composite action effect under hogging and sagging moments. Past recommendations for considering the composite slab effect in fully-rigid connections [57] may be applicable to partial-strength endplate connections, However, further experimental and numerical research is needed in this area.

The models capture the total rotation of the connection, including any potential shear deformations in the column web panel zone. Accordingly, as part of lumped plasticity models, a single rotation spring shall be used to idealize the connection. This spring can be allocated at the column flange face, offset from the column center using rigid beam elements. If a separate spring is to be used for the column web panel zone [9], the proposed backbone curves shall be modified first. This can be done by substituting larger values for the column-related predictors in the equations to implicitly remove the column impact on the stiffness and the strength of the connection.

The format of the proposed models is simple enough to be incorporated as part of numerical codes and in nonlinear modeling guidelines [5,6]. Furthermore, a computer tool with a friendly graphical user interface is developed and made publicly and downloadable from a GitHub repository [58]. Through this tool, the user can simply define the type and parameters of the connection and visualize the generated backbone curve and response parameter values (see demonstration video within the supplementary material).

8. Summary and conclusions

This paper describes the development of empirical backbone moment-rotation models for partial-strength flush (FEPC) and extended (EEPC) endplate steel connections, as part of beam-to-column joints. A large dataset, comprising both experimental and high-fidelity continuum finite element simulation data, was used for that purpose. Multivariate regression equations are provided for the definition of the backbone curve response parameters. The model is characterized by the following:

- The models capture the post-yield hardening, the failure point, and subsequent residual resistance after first bolt failure, which are commonly ignored in past models.
- Each model is complemented with statistical metrics to quantify the observed residual error variability. Those can be used to obtain the lower- and upper-bound backbone curves in support of probabilistic simulations and studies concerned with structural reliability.
- The models address the current need for accurate models for such connection types and pave the road towards the consideration of their structural contributions as part of system-level numerical studies.
- The model definition and simple empirical format are consistent with existing and established numerical modeling guidelines for steel structures [5,6,36] to allow for their potential adoption in engineering practice.
- Given their robust estimation of the elastic stiffness and plastic strength, the models can be used in standard design procedures and for the optimization of connection geometry to achieve target response characteristics.
- The models can be used to construct the fragility functions for the yielding and failure damage states. Those are useful for loss assessment studies as part of the performance-based design framework.
- The proposed models also demonstrate the level of stiffness, strength, and ductility that can be developed by endplate connections. Specifically, FEPCs and EEPCs can develop rotational stiffness as high as

17 and 55 times the beam's flexural rigidity, respectively. On average, FEPCs and EEPCs can also develop a plastic moment equal to 35 % and 55 % of that of the connected beam, respectively. These values will be potentially higher if a composite concrete slab is present. The relatively high stiffness and strength of endplate connections can also be coupled with appreciable ductility if properly detailed and fabricated. The connections demonstrated their ability to easily sustain rotations larger than 4 % rads before failure.

Notation

The following symbols are used in this paper:

d₁ bolt diameter

 d_{t} distance between the top bolt row and beam flange center in tension

E_b beam's Young's modulus

 $f_{y,\mathbf{i}}$ yield stress of component i [P: endplate, C: column, B: beam, b: bolt]

 $f_{\rm u,i}$ ultimate stress of component i [P: endplate, C: column, B: beam, b: bolt]

g bolt gauge length

 $h_{\rm b}$ beam depth

h_c column depth

 $I_{x,b}$ moment of inertia about the beam's strong axis

Ke elastic rotational stiffness

K_s post-yield hardening stiffness based on an equal-area bilinear fit

L_b beam length

max maximum value

min minimum value

M_c capping moment

 $M_{\rm p,b}$ the beam's plastic moment

 $M_{\rm res,c}$ residual moment for compression (last) bolt row

 $M_{\rm res,m}$ residual moment for middle bolt row

M_v yield moment

 M_{ye} effective yield (plastic) moment

p distance between the second bolt row in tension and the middle

 $p_{\rm t}$ pitch between bolt rows in tension above/below the beam flange P_{20} percentage of specimens with a prediction error within $\pm 20~\%$

 P_{50} percentage of specimens with a prediction error within $\pm 50~\%$

 R^2 coefficient of determination

 $t_{\rm cf}$ column flange thickness

 $t_{\rm cw}$ column web thickness

 $t_{\rm ep}$ endplate thickness

X input parameter *Y* output parameter

 β regression coefficient/exponent

 ε residual error

 $\varepsilon_{\mathrm{.rel}}$ residual relative error

 $\mu_{|\varepsilon,rel|}$ mean of the absolute residual relative error

 σ_{ϵ} standard deviation of the residual error

 $\sigma_{|\varepsilon,rel|}$; standard deviation of the absolute residual relative error

 $\theta_{\rm c}$ capping rotation

 $\boldsymbol{\theta}_{c,m}$ ultimate rotation after tensile bolt failure with middle bolts

 θ_{pc} post-capping rotation

 θ_u ultimate rotation after tensile bolt failure without middle bolts

 θ_y yield rotation

CRediT authorship contribution statement

Ahmed Elkady: Writing – review & editing, Visualization, Supervision, Software, Methodology, Funding acquisition, Conceptualization. Zizhou Ding: Writing – original draft, Visualization, Validation, Methodology, Investigation, Formal analysis, Data curation.

Declaration of Competing Interest

The authors declare that they have no known competing financial interests or personal relationships that could have appeared to influence the work reported in this paper.

Acknowledgements

This work was conducted at the National Infrastructure Laboratory, University of Southampton (UoS). The authors gratefully acknowledge the financial support provided by UoS to the first author as part of his studentship. The authors also acknowledge the use of the IRIDIS High Performance Computing Facility, and associated support services at the University of Southampton, in the completion of this work.

Appendix A. Supporting information

Supplementary data associated with this article can be found in the online version at doi:10.1016/j.engstruct.2025.121465.

Data availability

The experimental data used herein is made available through a public repository. Other data can be made available upon reasonable request.

References

- Ibarra L., Krawinkler H. Global collapse of frame structures under seismic excitations. Report No. 152 The John A Blume Earthquake Engineering Center, Stanford University, Stanford, CA: Stanford University, 2005.
- [2] Haselton C.B., Liel A.B., Lange S.T., Deierlein G.G. Beam-column element model calibrated for predicting flexural response leading to global collapse of RC frame buildings. Report No. 2007/03: Pacific Earthquake Engineering Research Center, Berkeley, CA, USA; 2008.
- [3] Lignos DG, Krawinkler H. Deterioration modeling of steel components in support of collapse prediction of steel moment frames under earthquake loading. J Struct Eng 2011;137(11). https://doi.org/10.1061/(ASCE)ST.1943-541X.0000376.
- [4] Hamburger R., Deierlein G.G., Lehman D.E., Lignos D.G., Lowes L.N., Pekelnicky R. et al. Recommended modeling parameters and acceptance criteria for nonlinear analysis in support of seismic evaluation, retrofit, and design NIST GCR 17-917-45: Prepared for the U.S. Department of Commerce and the National Institute of Standards and Technology (NIST) by the Applied Technology Council (ATC), 2018.
- [5] AISC. Seismic provisions for evaluation and retrofit of existing structural steel buildings. ANSI/AISC 342-22: American Institute for Steel Construction, Chicago, PIL; 2022.
- [6] ASCE. Seismic evaluation and retrofit of existing buildings. ASCE/SEI 41-23: American Society of Civil Engineers, Reston, VA.; 2023.
- [7] Lignos DG, Hartloper A, Elkady A, Deierlein GG, Hamburger R. Proposed updates to the ASCE 41 nonlinear modeling parameters for wide-flange steel columns in support of performance-based seismic engineering. J Struct Eng 2019;145(9). https://doi.org/10.1061/(ASCE)ST.1943-541X.0002353.
- [8] Karamanci E, Lignos DG. Computational approach for collapse assessment of concentrically braced frames in seismic regions. J Struct Eng 2014;140(SPECIAL: Computational Simulation in Structural Engineering). https://doi.org/10.1061/ (ASCE)ST.1943-541X.0001011.
- [9] Skiadopoulos A, Elkady A, Lignos DG. Proposed panel zone model for seismic design of steel moment-resisting frames. J Struct Eng 2021;147(4). https://doi.org/ 10.1061/(ASCE)ST.1943-541X.0002935.
- [10] Elkady A, Lignos DG. Effect of gravity framing on the overstrength and collapse capacity of steel frame buildings with perimeter special moment frames. Earthq Eng Struct Dyn 2015;44(8). https://doi.org/10.1002/eqe.2519.
- [11] Ding Z, Elkady A. Semirigid bolted end-plate moment connections: review and experimental-based assessment of available predictive models. J Struct Eng 2023; 149(9). https://doi.org/10.1061/JSENDH.STENG-11797.
- [12] Elkady A., Mak L. Data driven evaluation of existing numerical modelling guidelines for semi-rigid connections. 10th International Conference on Behaviour of Steel Structures in Seismic Areas (STESSA). Timisoara, Romania: Springer International Publishing; 2022.
- [13] Murray T.M., Sumner E.A. Extended end-plate moment connections: Seismic and wind applications. Design Guide 4: American Institute of Steel Construction, Chicago, Illinois, USA; 2003.
- [14] Murray T.M., Shoemaker W.L. Flush and extended multiple-row moment end-plate connections. Design Guide 16: American Institute of Steel Construction, Chicago, Illinois, USA; 2002.

- [15] Kidd M, Judge R, Jones SW. Current UK trends in the use of simple and/or semirigid steel connections. Case Stud Struct Eng 2016;6. https://doi.org/10.1016/j. csse 2016.05.004
- [16] Flores FX, Charney FA, Lopez-Garcia D. Influence of the gravity framing system on the collapse performance of special steel moment frames. J Constr Steel Res 2014; 101:0. https://doi.org/10.1016/j.jcsr.2014.05.020.
- [17] Hwang SH, Lignos DG. Effect of modeling assumptions on the earthquake-Induced losses and collapse risk of steel-frame buildings with special concentrically braced frames. J Struct Eng 2017;143(9). https://doi.org/10.1061/(ASCE)ST.1943-541X.0001851.
- [18] Elkady A. Response characteristics of flush end-plate connections. Eng Struct 2022; 269. https://doi.org/10.1016/j.engstruct.2022.114856.
- [19] Elkady A, Lignos DG. Full-scale testing of deep wide-flange steel columns under multi-axis cyclic loading: loading sequence, boundary effects and out-of-plane brace force demands. ASCE J Struct Eng 2018;144(2). https://doi.org/10.1061/ (ASCE)ST.1943-541X.0001937.
- [20] Cravero J, Elkady A, Lignos DG. Experimental evaluation and numerical modeling of wide-flange steel columns subjected to constant and variable axial load coupled with lateral drift demands. J Struct Eng 2020;146(3). https://doi.org/10.1061/ (ASCE)ST.1943-541X.0002499.
- [21] Krawinkler H. Cyclic loading histories for seismic experimentation on structural components. Earthq Spectra 1996;12(1). https://doi.org/10.1193/1.1585865.
- [22] Shi G, Shi Y, Wang Y. Behaviour of end-plate moment connections under earthquake loading. Eng Struct 2007;29(5). https://doi.org/10.1016/j. engstruct 2006.06.016
- [23] Mak L, Elkady A. Experimental database for steel flush end-plate connections. J Struct Eng 2021;147(7). https://doi.org/10.1061/(ASCE)ST.1943-541X 0003064
- [24] Benterkia Z. End-plate connections and analysis of semi-rigid steel frames. Coventry, UK: University of Warwick; 1991.
- [25] Weynand K., Huter M., Kirby P., da Silva L.A.P., Cruz P.J.S. SERICON A Databank for tests on semi-rigid joints. COST C1: Control of the Semi-Rigid Behavior of Civil Engineering Structural Connections: Office for Official Publications of the European Communities; 1999.
- [26] ABAQUS-FEA/CAE. Dassault Systemes Simulia Corp., RI, USA. © Dassault Systemes, 2010, 2011.
- [27] Huang J. Stress-strain models for carbon steels: University of Macau; 2010.
- [28] Ding Z, Elkady A. Generalized spring model for steel bolts in tension considering uncertainty and loading speed. J Constr Steel Res 2025;231. https://doi.org/ 10.1016/j.jcsr.2025.109574.
- [29] Elkady A, Lignos DG. Analytical investigation of the cyclic behavior and plastic hinge formation in deep wide-flange steel beam-columns. Bull Earthq Eng 2015;13 (4). https://doi.org/10.1007/s10518-014-9640-y.
- [30] Newell J.D., Uang C.-M. Cyclic behavior of steel columns with combined high axial Load and drift demand. Report No. SSRP-06/22: Department of Structural Engineering, University of California, San Diego, 2006.
- [31] Rölle L. The load-bearing and deformation behavior of bolted steel and composite joints in fully plastic design and in extraordinary design situations (in german). Stuttgart, Germany: University of Stuttgart; 2013.
- [32] Augusto H, Simões da Silva L, Rebelo C, Castro JM. Characterization of web panel components in double-extended bolted end-plate steel joints. J Constr Steel Res 2016;116. https://doi.org/10.1016/j.jcsr.2015.08.022.
- [33] Menegotto M, Pinto PE. Method of analysis for cyclically loaded RC frames including changes in geometry and non-elastic behaviour of elements under combined normal force and bending. IABSE Congr Rep Work Comm 1973.
- [34] Richard RM, Abbott BJ. Versatile elastic-plastic stress-strain formula. J Eng Mech Div 1975;101(4). https://doi.org/10.1061/JMCEA3.0002047.
- [35] Ibarra LF, Medina RA, Krawinkler H. Hysteretic models that incorporate strength and stiffness deterioration. Earthq Eng Struct Dyn 2005;34(12). https://doi.org/ 10.1002/ege.495.

- [36] NIST. Guidelines for nonlinear structural analysis for design of buildings Part IIa Steel MRFs. NIST GCR 17-917-46v2: NEHRP consultants Joint Venture, 2017.
- [37] FEMA. Seismic performance assessment of buildings. Report FEMA P-58-1: Federal Emergency Management Agency, Washington, DC, 2012.
- [38] Kozlowski A., Kowalczyk R., Gizejowski M. Estimation of the initial stiffness and moment resistance of steel and composite joints. 8th World Congress, Council on Tall Buildings and Urban Habitat (CTBUH). Dubai, United Arab Emirates: Council on Tall Buildings and Urban Habitat (CTBUH), Illinois, USA.; 2008.
- [39] Eladly MM, Schafer BW. Numerical and analytical study of stainless steel beam-to-column extended end-plate connections. Eng Struct 2021;240. https://doi.org/10.1016/j.engstruct.2021.112392.
- [40] Georgiou G, Elkady A. ANN-based model for predicting the nonlinear response of flush endplate connections. ASCE J Struct Eng 2024;150(5). https://doi.org/ 10.1061/JSENDH/STENG-13119.
- [41] Menard S. Applied logistic regression analysis. Thousand Oaks, CA: Sage; 2002.
- 42] Chatterjee S., Hadi A.S. Regression analysis by example. Fifth Edition ed: John Wiley & Sons; 2015.
- [43] Lilliefors HW. On the Kolmogorov-Smirnov test for normality with mean and variance unknown. J Am Stat Assoc 1967;62(318). https://doi.org/10.2307/ 2283970
- [44] Breusch TS, Pagan AR. A simple test for heteroscedasticity and random coefficient variation. Économ J Econom Soc 1979;47(5). https://doi.org/10.2307/1911963.
- [45] Mann A.P., Morris L.J. Significance of lack of fit-flush beam-column connections. Joints in structural steelwork: Pentech Press, London; 1981.
- [46] Jaspart J.-P., Maquoi R. Effect of bolt preloading on joint behaviour. 1st European Conference on Steel Structures. Athens, Greece, 1995.
- [47] Tartaglia R, D'Aniello M, Zimbru M. Experimental and numerical study on the T-Stub behaviour with preloaded bolts under large deformations. Structures 2020;27. https://doi.org/10.1016/j.istruc.2020.08.039.
- [48] AISC. Specifications for structural steel buildings. ANSI/AISC 360-22: American Institute for Steel Construction, Chicago, P.I.; 2022.
- [49] CEN. Eurocode 3 Design of steel structures, Part 1-1: General rules and rules for buildings. BS-EN 1993-1-1-2006: European Committee for Standardization, Brussels, Belgium; 2005.
- [50] Eatherton M.R., Nguyen T.N., Murray T.M. Yield line patterns for end-plate moment connections. Report No. CE/VPI-ST-21/05: Virginia Polytechnic Institute and State University, Blacksburg, VA, USA; 2021.
- [51] CEN. Eurocode 3 Design of steel structures, Part 1-8: Design of joints. BS-EN 1993-1-8-2006: European Committee for Standardization, Brussels, Belgium; 2005.
- [52] Ostrander J.R. An experimental investigation of end plate connections. Saskatchewan, Canada: University of Saskatchewan; 1970.
- [53] Jenkins WM, Tong CS, Prescott AT. Moment-transmitting endplate connections in steel construction, and a proposed basis for flush endplate design. Struct Eng 1986; 64:5 (doi).
- [54] Sherbourne AN, Bolted beam-to-column connections, Struct Eng 1961:39:6 (doi).
- [55] Tong C.S. The elastic-plastic behaviour of semi-rigid connections in steel structures. Hatfield, UK Hatfield Polytechnic; 1985.
- [56] Prinz GS, Nussbaumer A, Borges L, Khadka S. Experimental testing and simulation of bolted beam-column connections having thick extended end plates and multiple bolts per row. Eng Struct 2014;59. https://doi.org/10.1016/j. engstruct.2013.10.042.
- [57] Elkady A, Lignos DG. Modeling of the composite action in fully restrained beam-to-column connections: rlmplications in the seismic design and collapse capacity of steel special moment frames. Earthq Eng Struct Dyn 2014;43(13). https://doi.org/10.1002/eng-2430
- [58] A. Elkady EPC backbone app, GitHub United Kingdom; 2025. (https://Github.com/Amaelkady/SRConED/Tree/Main/EPC Backbone Model).